J. Wind Eng. Ind. Aerodyn. 104–106 (2012) 116–128

Contents lists available at SciVerse ScienceDirect

Journal of Wind Engineering and Industrial Aerodynamics

journal homepage: www.elsevier.com/locate/jweia

Performance evaluation of Canton Tower under winds based on full-scale data

Y.L. Guo [a,*], A. Kareem [a], Y.Q. Ni [b], W.Y. Liao [b]

[a] University of Notre Dame, 156 Fitzpatrick Hall, Notre Dame, IN 46556, USA
[b] Department of Civil and Structural Engineering, The Hong Kong Polytechnic University, Kowloon, Hong Kong, China

ARTICLE INFO

Available online 20 April 2012

Keywords:
Wind effects
Typhoon
Structural health monitoring
Full-scale data
Tall towers
Wind characteristics
Structural dynamics
Turbulence

ABSTRACT

Canton Tower is a 610 m tall tower, located at the edge of the most active typhoon prone area in the world. Therefore, the wind effects are critical to the satisfactory performance of the tower. Although the finite element analysis and wind tunnel tests have been conducted in response to this concern, the full-scale monitoring provides a unique opportunity to study the actual performance of the structure under winds. A sophisticated long-term Structural Health Monitoring system consisting of about 700 sensors has been implemented by The Hong Kong Polytechnic University. This paper presents wind characteristics (wind speed, direction, and turbulence intensity) and structural responses (strain, acceleration, and displacement responses) during several typhoon events. A comparison between the full-scale data and wind tunnel predictions is conducted. Prior to modal identification, stationarity check is conducted and then different techniques are employed to identify the modal properties with errors. In addition, the amplitude-dependence in modal properties is investigated. Finally, the tower serviceability during different typhoon events is evaluated and the performance is found to be satisfactory from human comfort consideration.

1. Introduction

Canton Tower, located in the city of Guangzhou, China, is a 610 m tall tower, consisting of an inner reinforced concrete structure and an outer steel lattice structure, as shown in Fig. 1(a). There are 37 floors linking the inner and outer structures for various functions including TV and radio transmission facilities, observatory decks, revolving restaurants, computer gaming, restaurants, exhibition spaces, conference rooms, shops and 4D cinemas.

Guangzhou is located at the edge of the most active typhoon prone area in the world, therefore the wind effects play a major role in overall performance of the tower. The 100-year and 10-year design wind speeds in the area are 10-min mean wind speeds of 52.4 m/s and 38.7 m/s respectively at the gradient height (400 m) (GBJ9-Department of Standards and Norms, 1994). The finite element (FE) analysis combined with wind tunnel tests has been conducted to study the effects of wind on the tower. However, these analyses are solely based on the analytical and scaled models, which necessitates that the accuracy and validity of the results be calibrated with respect to the observed performance (Kijewski-Correa et al., 2006). Therefore, full-scale monitoring becomes the most important means for performance evaluation of tall structures under winds.

Although the strong motion monitoring system for seismic applications have been widely reported (more than 150 buildings in California, USA, more than 100 buildings in Japan, and more than 40 buildings in Taiwan have been instrumented with seismic monitoring system (Huang, 2006; Kijewski-Correa and Kareem, 2003; Lin et al., 2003)), full-scale measurements under strong winds are not as widespread as those for seismic. Xu and Zhan (2001) conducted a two and a half months field measurement for the 384 m high Di Wang Tower. The wind properties and structural responses during Typhoon York in 1999 were measured and analyzed. A long-term monitoring program has been initiated by the University of Notre Dame (Kijewski-Correa and Kareem, 2003; Kijewski-Correa et al., 2006). In this study, full-scale measurements have been compared to wind tunnel based predictions and the FE analysis commonly used in design. Li and his co-investigators have made full-scale measurements for several high-rise structures under strong winds (e.g. Li et al., 2004; Li et al., 2008).

A sophisticated long-term Structural Health Monitoring (SHM) system consisting of about 700 sensors (sensors for monitoring wind properties and structural response shown in Fig. 1(b–e)) has been implemented in Canton Tower by The Hong Kong Polytechnic University (Ni et al., 2011, 2009). This system is one of few

* Corresponding author. Tel.: +1 574 631 2540; fax: +1 574 631 9236.
E-mail addresses: yguo1@nd.edu (Y.L. Guo), kareem@nd.edu (A. Kareem), Yiqing.Ni@inet.polyu.edu.hk (Y.Q. Ni), weiyang.liao@polyu.edu.hk (W.Y. Liao).

0167-6105/$ - see front matter © 2012 Elsevier Ltd. All rights reserved.
http://dx.doi.org/10.1016/j.jweia.2012.04.001

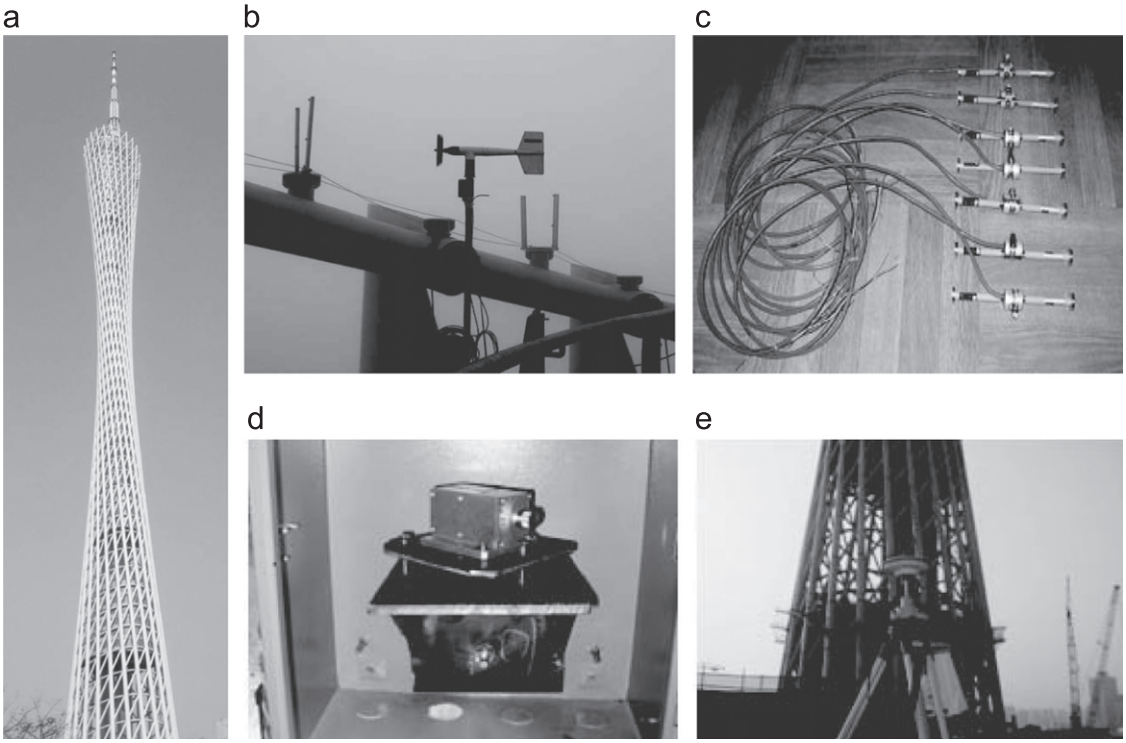

Fig. 1. Canton Tower and sensors used for monitoring wind properties and structural responses: (a) Canton Tower, (b) anemometer, (c) vibrating wire gauge, (d) accelerometer, and (e) global positioning system (GPS).

SHM practices that integrate in-construction and in-service monitoring. The analysis of measured full-scale data as well as the FE modeling have been reported in Chen et al. (2011). This paper will provide a different perspective on the measurement data. The analysis of wind properties of recent typhoon events (i.e. Typhoon Sarika, Typhoon Haima, and Typhoon Nock-ten) in 2011 is detailed. The structural responses, e.g. strain, acceleration, displacement, measured during both the recent and previous typhoon events which occurred in 2008 and 2009 are reported. A comparison between the full-scale data and wind tunnel prediction is conducted. For modal identification, stationarity check is conducted in order to guarantee reliable system identification. Different techniques are employed to identify modal properties and associated errors are discussed. In addition, the amplitude-dependence in the modal properties is examined. Finally, the tower serviceability during different typhoon events is evaluated.

2. Full-scale data measured during typhoon events

2.1. Wind properties

One anemometer (RM Youngh, 05103 L) was installed at the height of 461.1 m, as shown in Fig. 1(b). The measurement range of the anemometer is 0∼100 m/s and output signal is electric current type so that the signal can be transmitted to the data acquisition unit about 100 m away. Wind direction and speed are continuously recorded at a sampling frequency of 50 Hz. The data measured during typhoon events were extracted for analysis. Fig. 2 shows the 10-min mean wind speed and direction (0° denotes north direction, an arbitrary direction is measured from the north in a clockwise direction) measured during Typhoon Sarika (June 10, 2011), Typhoon Haima (June 22, 2011) and Typhoon Nock-ten (July 29, 2011). The measured maximum 10-min mean wind speeds for Typhoon Sarika, Typhoon Haima and Typhoon Nock-ten at the tower site are 5.0 m/s, 14.8 m/s, and 11.9 m/s respectively. The maximum 3-s mean wind speeds for the three typhoon events are 9.7 m/s, 17.6 m/s and 16.8 m/s. Note that 10-min mean wind speed and 3-s wind speed are calculated by taking the average of data segments of 10 min and 3 s duration, respectively. The observed wind speeds are lower than the design wind speeds. Those observations were obtained only in recent years, which cannot be conclusive whether the design wind speed is conservative or not. The long-term monitoring should be continued to obtain statistical data of wind speeds to arrive at a more definitive conclusion.

The time histories of wind speeds and directions are divided into 10-min segments. For each segment, the measured wind speed can be decomposed into longitudinal component $U(t)=U+u(t)$ and lateral component $w(t)$, where U is the mean wind speed, $u(t)$is the longitudinal fluctuating component. $U(t)$, U, as well as $\pm\sigma_u$ (standard deviation of $u(t)$) of Typhoon Haima (21:00–21:10 Beijing time, on June 22, 2011) are shown in Fig. 3(a), while the corresponding $w(t)$ and $\pm\sigma_w$ (standard deviation of $w(t)$) are shown in Fig. 3(b).

The longitudinal turbulence intensity is readily defined by

$$I_u = \frac{\sigma_u}{U} \tag{1}$$

The longitudinal turbulence intensity for Typhoon Sarika, Typhoon Haima, and Typhoon Nock-ten are shown in Fig. 4. It is seen from Fig. 4(a) that when wind speed is greater than 4 m/s, the turbulence intensity is below 20% for Typhoon Sarika. For low wind speed, turbulence intensity is typically high, similar observation has been reported by others (Wu et al., 2011). For Typhoon Haima, a decreasing trend for turbulence intensity with the increase of the mean wind speed is observed in Fig. 4(b), and the turbulence intensity for different mean wind speeds mainly fluctuates between 10% and 20%. In Fig. 4(c), it is noted that the 10-min mean wind speeds mainly varies between 8 m/s and 8.5 m/s for Typhoon Nock-ten and the corresponding turbulence intensity is around 12%. It is also noted that for both Typhoon

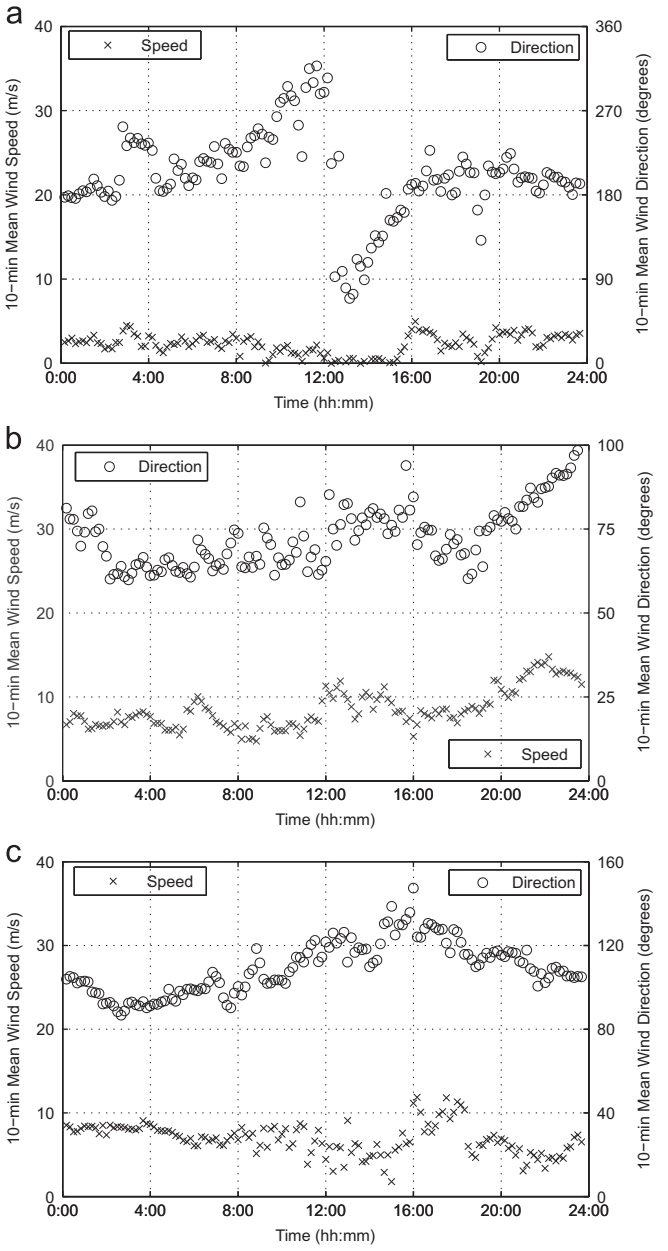

Fig. 2. 10-min mean wind speed and direction measured: (a) Typhoon Sarika, June 10, 2011, (b) Typhoon Haima, June 22, 2011, and (c) Typhoon Nock-ten, July 29, 2011.

Haima and Typhoon Nock-ten, when wind speed is higher than 10 m/s, turbulence intensity tends to remain constant. The corresponding mean turbulence intensities during the two typhoon events are 13.2% and 13.8%, respectively; and the corresponding mean turbulence length scales are 118.1 m and 248.4 m, respectively. For Typhoon Sarika, turbulence intensity tends to remain constant when wind speed is higher than 4 m/s. The corresponding mean turbulence intensity and length scale are 13.7% and 73.4 m. The turbulence intensity profile assumed in wind tunnel test is given by (Zhu et al., 2006)

$$I_u = 0.1 \cdot \left(\frac{Z}{Z_g}\right)^{-0.27} \tag{2}$$

where Z is height, Z_g is gradient height. According to the above equation, I_u at 461.1 m is 9.6%. For this set of measurement, the

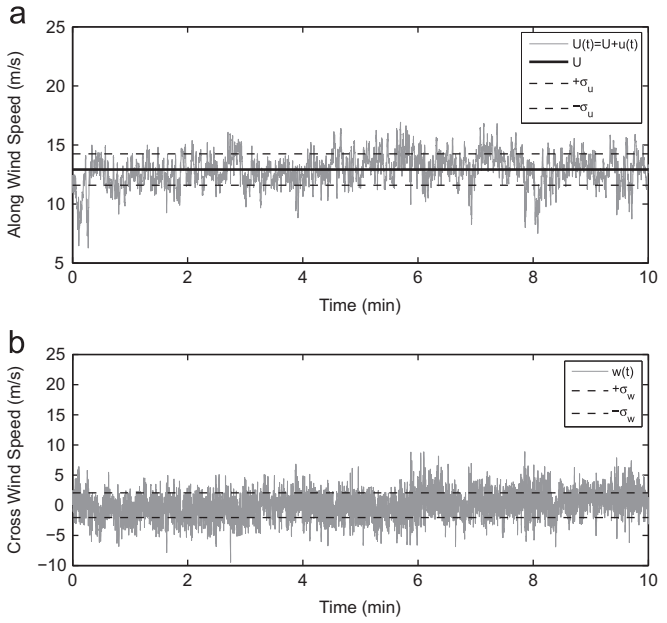

Fig. 3. 10-min time histories for longitudinal and lateral wind speed measured during Typhoon Haima on June 22, 2011, 21:00-21:10 Beijing time: (a) longitudinal wind speed, and (b) lateral wind speed.

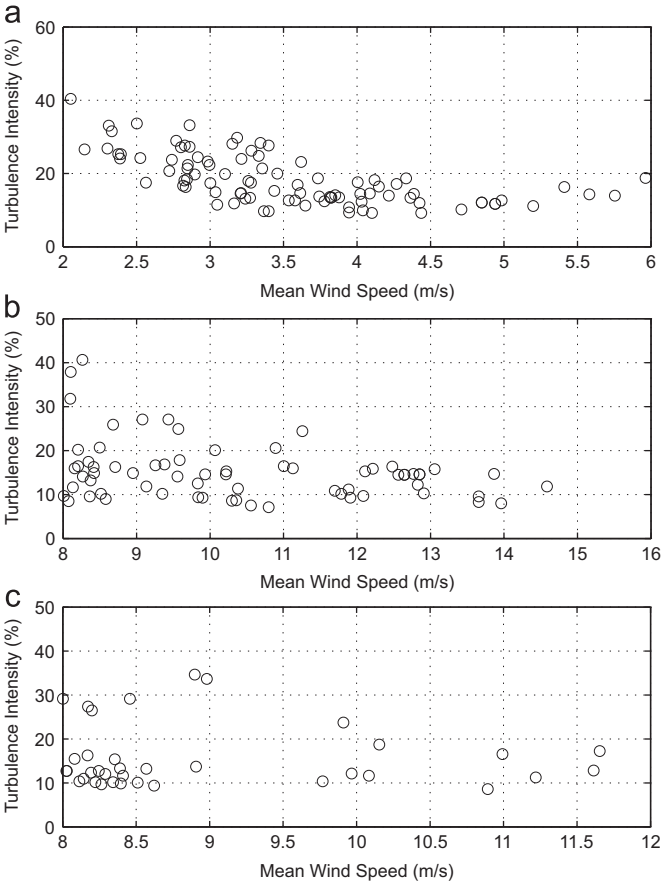

Fig. 4. Longitudinal wind turbulence intensity: (a) Typhoon Sarika, (b) Typhoon Haima, and (c) Typhoon Nock-ten.

turbulence intensities in the field are 40% higher than those assumed in the wind tunnel test. The scatter in turbulence intensity is generally high at low wind speeds due to the scatter in data. Therefore, such a deviation is quite plausible.

According to the classification method of atmospheric turbulence proposed by Pasquill (1974), the atmospheric stratification is neutral when wind speed is greater than 6 m/s. Therefore, the influence atmospheric of stratification on turbulence is not significant for Typhoon Haima and Typhoon Nock-ten. However, for Typhoon Sarika, when wind speed is between 2 and 5 m/s, the atmospheric stratification is unstable in day time and neutral or stable in night time; and when wind speed is larger than 6 m/s, the atmospheric stratification is neutral. Thus atmospheric stratification plays a more important role in turbulence intensity in Typhoon Sarika than in Typhoons Haima and Nock-ten. This may contribute to the more frequently observed high turbulence intensities (greater than 20%) in Typhoon Sarika than in Typhoons Haima and Nock-ten (see Fig. 4). As mentioned earlier, the scatter in turbulence is more prevalent at low wind speed which may be a source of this high level of turbulence intensity.

It is noted that the turbulence intensity is also heavily influenced by the wind direction. For turbulence intensities, which are higher than 20%, the mean values of the standard deviation of wind direction are 25.6°, 20.5° and 25.2° for Typhoon Sarika, Typhoon Haima and Typhoon Nock-ten, respectively, while for turbulence intensities, which are lower than 20%, the mean values are 10.5°, 10.3° and 9.8° for the three typhoon events. This suggests that large fluctuation in wind direction is another source of high turbulence intensity in full-scale observations.

2.2. Strain measurements

Based on the preliminary results of FE analysis, 12 levels (at elevations of 32.8 m, 100.4 m, 121.2 m, 173.2 m, 204.4 m, 230.4 m, 272.0 m, 303.2 m, 334.4 m, 355.2 m, 376.0 m, and 433.2 m) of the tower with high stress were chosen for strain monitoring during both the in-construction and in-service stages. Four vibrating-wire strain gauges were embedded into reinforced concrete wall at these levels of the inner structure. A typical layout of the measurement points in relation to the cross-section of the inner structure is shown in Fig. 5. When observing the measured vertical strains of point 2 and point 4 on the cross-section at level 121.2 m high during the Typhoon Neoguri (April 19, 2008), it was noted that large strain variations occurred between 18:00 and 19:00 (Beijing time) when the wind speed reached the maximum value. It was also observed that the vertical compressive strain decreases at point 2 and increased at point 4 because the Typhoon Neoguri winds were mainly from east to west. The maximum stress variation during Typhoon Neoguri (April 19, 2008), Typhoon Kammuri (August 6, 2008), Typhoon Nuri (August 22, 2008), and Typhoon Hagupit (September 24, 2008) is approximately 0.5 MPa, which is about 20% of the static stress produced by the self-weight of the structure.

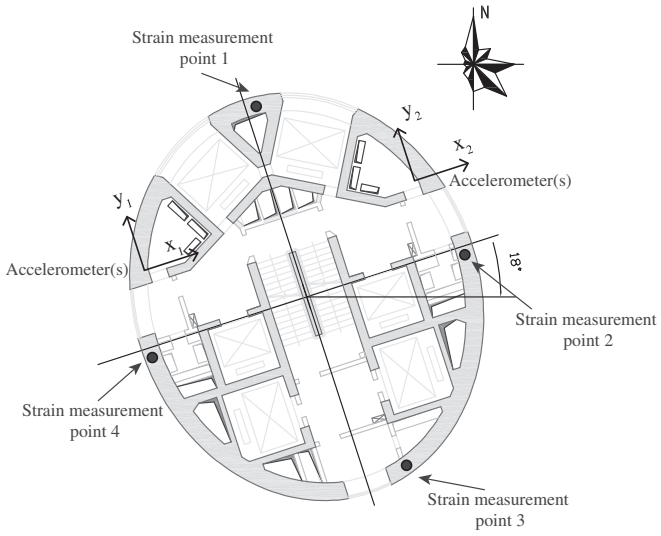

Fig. 5. Layout of strain measurement points and accelerometers.

2.3. Acceleration responses

20 uni-axial accelerometers (Tokyo Sokushin AS-2000C) were installed at eight levels (at elevations of 30.6 m, 119.3 m, 171.1 m, 228.5 m, 275.3 m, 332.2 m, 384.2 m, and 446.8 m) of the inner structure to monitor the acceleration response. The frequency response of the accelerometers ranges from DC-50 Hz (3 dB), the amplitude range is ± 2 g, and the sensitivity is 1.25 V/g. The 4th level and 8th levels were equipped with four uni-axial accelerometers, two for measurement of the horizontal acceleration along the short-axis of the inner structure (x_1 and x_2 shown in Fig. 5) and the other two for the long-axis (y_1 and y_2 shown in Fig. 5). The torsional acceleration can then be obtained by using accelerations measured in y_1 and y_2 directions. At the remaining six levels, each cross-section was equipped with two uni-axial accelerometers, one along the short-axis of the inner structure (x_1 shown in Fig. 5) and the other along the long-axis of the inner structure (y_2 shown in Fig. 5). Note that x- and y-directions are used to refer to the short-axis and long-axis of the inner structure, respectively. The sensors were mounted firmly to the shear wall of the inner structure via steel angles. Orientation of each accelerometer was determined by the positioned bolts that have been located accurately before installation. After calibrating the orientation, the sensors were locked in a steel box for protection. To reduce the noise due to long cables in conventional centralized data acquisition system, a specially designed de-centralized system was introduced, which also accounted for data synchronization. At each level, an acquisition unit was employed to collect the acceleration data from the 2 (or 4) sensors at this level. The total eight acquisition units were connected in series via two cables, one for synchronization and the other for acceleration data transmission. One PC placed in the tower was responsible for sending synchronization signal and collecting acceleration data. A bandwidth filter of 0.05 Hz to 40 Hz was designed for each acquisition unit. The system has 24 bit A/D converters. The sampling frequency of the acceleration measurement was 50 Hz.

The maximum accelerations measured at different levels during Typhoon Hagupit, Typhoon Haima, and Typhoon Nock-ten are shown in Fig. 6. It is seen that the maximum accelerations in x- and y-directions for Typhoon Hagupit are close to each other at different levels, and the maximum acceleration for all levels is 0.0414 m/s^2, which occurred in x-direction at the level 384.2 m. For Typhoon Haima, the maximum accelerations in x- and y-directions differed a lot at most levels except for levels at 119.3 m and 332.2 m. The maximum acceleration for all levels was 0.0164 m/s^2 and occurred in x-direction at the level 446.8 m. For Typhoon Nock-ten, the maximum accelerations in x-direction were much higher than those in y-direction for higher levels. The maximum acceleration for all levels was 0.0197 m/s^2, which was measured in x-direction at 446.8 m. The maximum accelerations for all these three typhoon events occurred in x-direction, which suggests that the structural stiffness in the y-axis is greater than that in the x-axis.

The power spectral density (PSD) of accelerations measured at different levels during Typhoon Haima is shown in Fig. 7. It is noted that the vibration modes in x- and y-directions are highly coupled, especially for the first five modes. The first vibration mode is dominant in the PSD of x-direction for higher levels (levels above 119.3 m), while for the levels 30.6 m and 119.3 m,

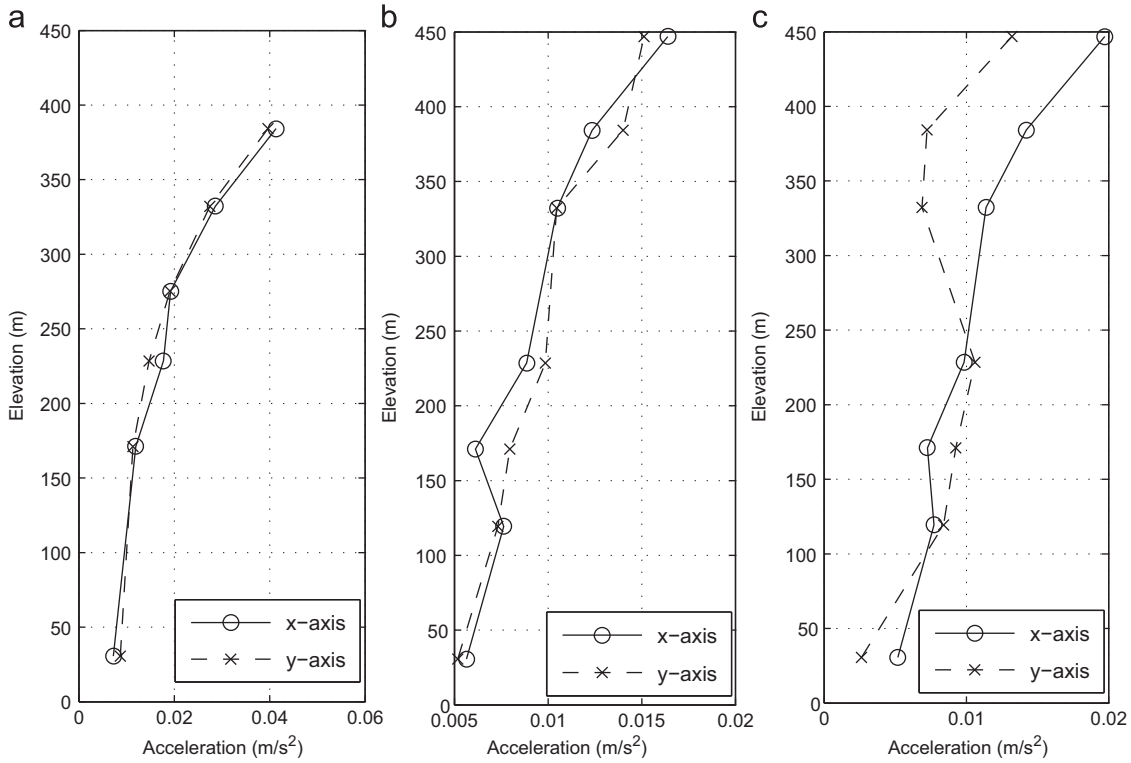

Fig. 6. Maximum accelerations measured during typhoons: (a) Typhoon Hagupit, (b) Typhoon Haima, and (c) Typhoon Nock-ten.

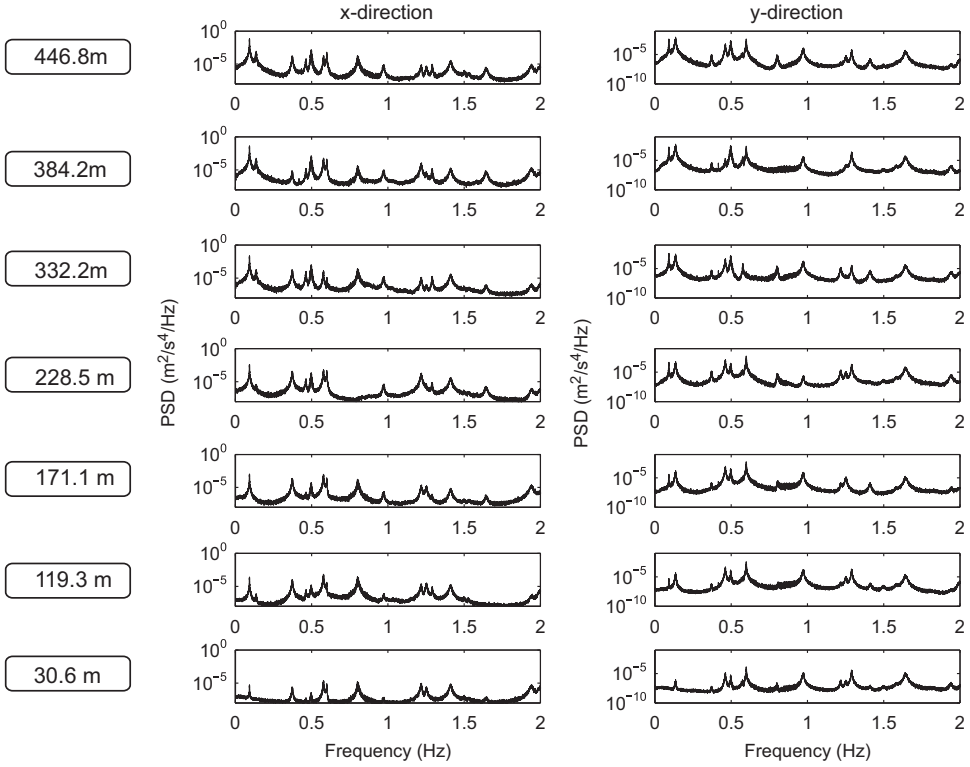

Fig. 7. Power spectral density of accelerations measured at different levels during Typhoon Haima.

the sixth mode is dominant. For the PSD in *y*-direction, the second vibration mode is dominant for levels at 446.8 m and 384.2 m, the first mode is dominant at level 332.2 m, and the sixth mode is dominant for all the other lower levels. The first mode can then be regarded as the first mode for *x*-direction, while the second mode can be viewed as the first mode for *y*-direction. Although not shown here due to the limitation of space, the first mode for torsion is the fifth mode.

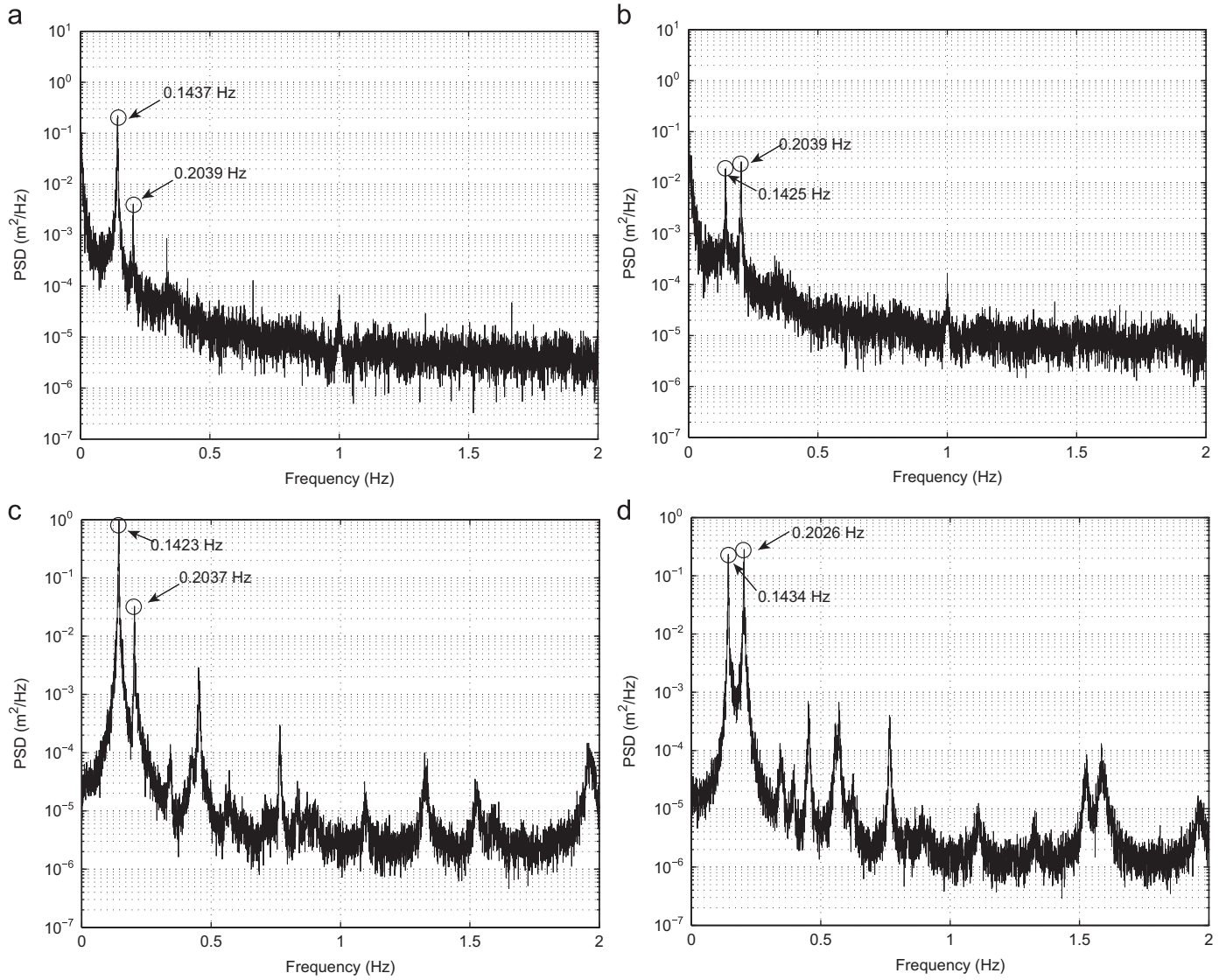

Fig. 8. Comparison between PSD of displacements and accelerations measured during Typhoon Nuri: (a) PSD of displacement in *x*-direction, (b) PSD of displacement in *y*-direction, (c) PSD of acceleration in *x*-direction, and (d) PSD of acceleration in *y*-direction.

2.4. Displacement responses

To monitor the displacement of the tower, a GPS system was deployed with a rover station at the tower top (454.0 m) and a reference station at the podium level. The sampling frequency is 5 Hz. The maximum displacement during Typhoon Neoguri, Typhoon Kammuri, Typhoon Nuri, and Typhoon Hagupit was measured to be approximately 15 cm. The comparison between the PSD of displacement and acceleration responses measured during Typhoon Nuri is shown in Fig. 8. The first two modal frequencies identified from the PSD of displacements in *x*-direction are 0.1437 Hz and 0.2039 Hz, which show a good agreement with those (0.1423 Hz and 0.2037 Hz) identified from the corresponding PSD of accelerations. The comparison of modal frequencies identified from the PSD of displacements and accelerations in *y*-direction shows similar results, as seen in Fig. 8. It is also observed from Fig. 8(b, d) that in comparison with the displacement PSD, the acceleration PSD exhibit more peaks in high frequency range as one could expect, from which the higher modes of the structure can be identified.

3. Comparison between wind tunnel test data and full-scale data

The acceleration response of the tower measured in typhoon events is compared to that obtained in the wind tunnel test. The wind tunnel test of full tower aeroelastic model was conducted in TJ-2 Boundary Layer Wind Tunnel at Tongji University (Zhu et al., 2007). The length scale λ_L used in the wind tunnel was 1:266, the frequency scale λ_f was 47:1. The velocity scale λ_u can be calculated from λ_L and λ_f, using the following relationship

$$\frac{f_F \cdot D_F}{U_F} = \frac{f_M \cdot D_M}{U_M} \tag{3}$$

where f_F, D_F, U_F are fundamental frequency, characteristic length, and wind velocity in full-scale; and f_M, D_M, U_M are fundamental frequency, characteristic length, and wind velocity in wind tunnel test.

Thus, λ_u is given by

$$\lambda_u = \frac{U_M}{U_F} = \frac{f_M}{f_F} \cdot \frac{D_M}{D_F} = \lambda_f \cdot \lambda_L \tag{4}$$

According to Eq. (4), velocity scale λ_u was 1:5.66. The wind velocity in wind tunnel test has been converted to the corresponding full scale wind velocity according to

$$U_F = U_M/\lambda_u \tag{5}$$

and given in wind tunnel test report (Zhu et al., 2006). The sensors were installed in three cross-sections (located at the heights corresponding to 278 m, 355 m and 443 m of the tower) of the main tower and one cross-section of the mast. Three miniature accelerometers were installed in each section of the main tower to measure the two translational acceleration and tortional acceleration; two miniature accelerometers were installed in the section of the mast to measure the two translational accelerations. The RMS and maximum acceleration responses measured for different wind directions corresponding to 100-year and 10-year design wind speeds are presented in Zhu et al. (2006). The 100-year and 10-year design wind speeds are 10-min mean wind speeds of 52.4 m/s and 38.7 m/s respectively at the gradient height (400 m) (GBJ9-Department of Standards and Norms, 1994). The full scale accelerations are measured at low wind speeds. In order to make comparison, RMS accelerations corresponding to these wind speeds in wind the tunnel test are estimated by using linear regression.

The anemometer in the SHM system was installed at the height of 461.1 m. The boundary layer in the wind tunnel test is modeled by assuming the gradient height as 400 m according to GBJ9-Department of Standards and Norms (1994). Based on the terrain characteristics, the wind speed at the height of 461.1 m is the same as that at the gradient height in the wind tunnel test. Therefore, the measured wind speeds in the field is compared to the gradient height wind speed in wind tunnel test. The measured wind speeds, directions and accelerations during one typhoon event are divided into 10-min data segments; then the 10-min mean of wind speeds and directions, the RMS of accelerations are calculated for each segment. Following this, the 10-min mean wind directions which are close to one of wind directions tested in the wind tunnel are selected and the corresponding 10-min mean wind speeds and RMS accelerations are extracted for comparison purpose. The selected wind speeds and directions for Typhoon Haima and Typhoon Nock-ten are shown in Fig. 9(a) and Fig. 10(a). It is seen that the wind directions selected during Typhoon Haima correspond to wind direction of 67.5° in the wind tunnel test, while the wind directions selected during Typhoon Nock-ten correspond to wind direction of 112.5° in the wind tunnel test.

It is seen from Fig. 9(b), (c) and (d) that the RMS of the measured accelerations in *x*- and *y*-directions scatter considerably,

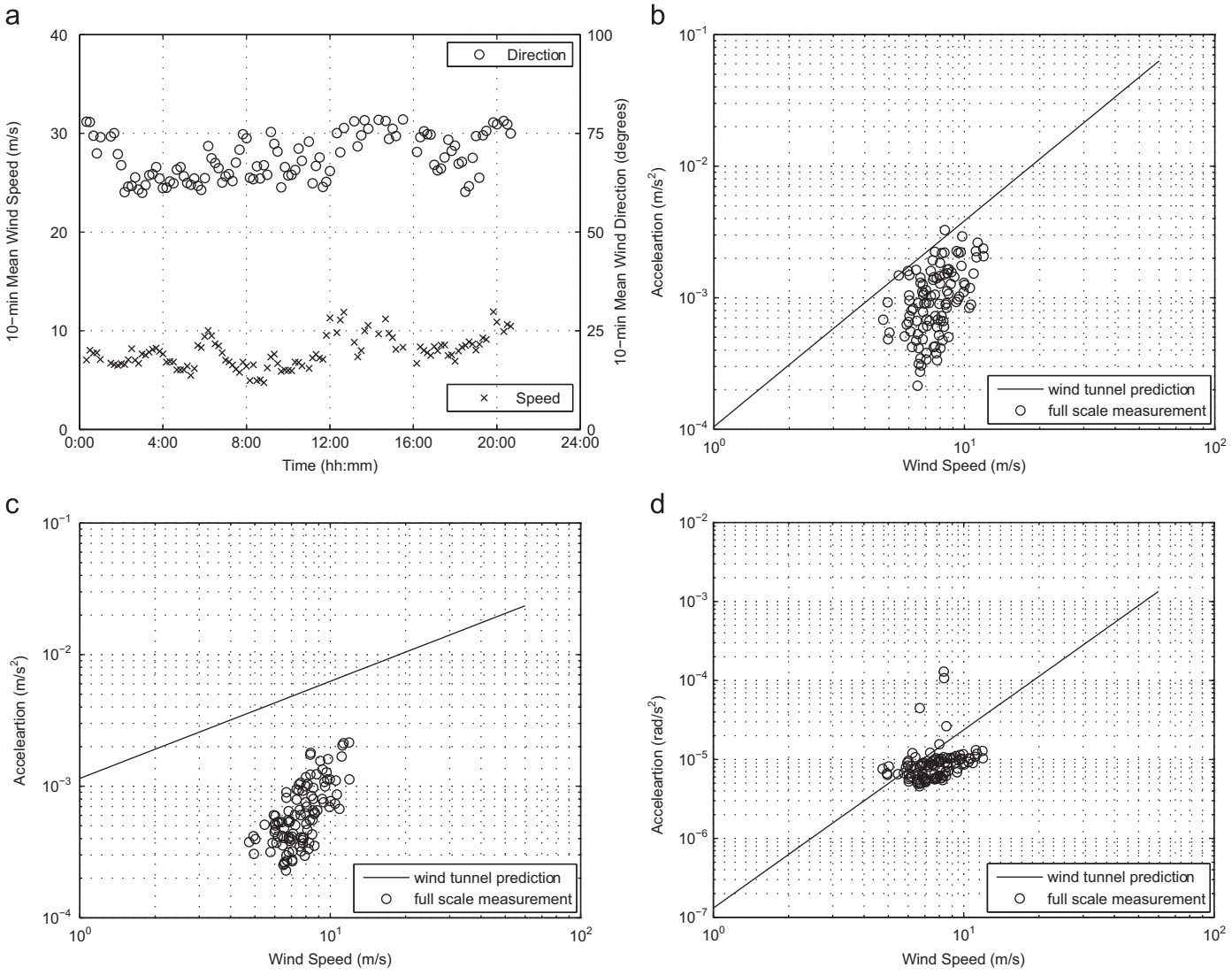

Fig. 9. Comparison between estimated RMS acceleration from wind tunnel test and measured RMS acceleration during Typhoon Haima, June 22, 2011: (a) selected 10-min mean wind speeds and wind directions, (b) *x*-direction, (c) *y*-direction, and (d) torsional direction.

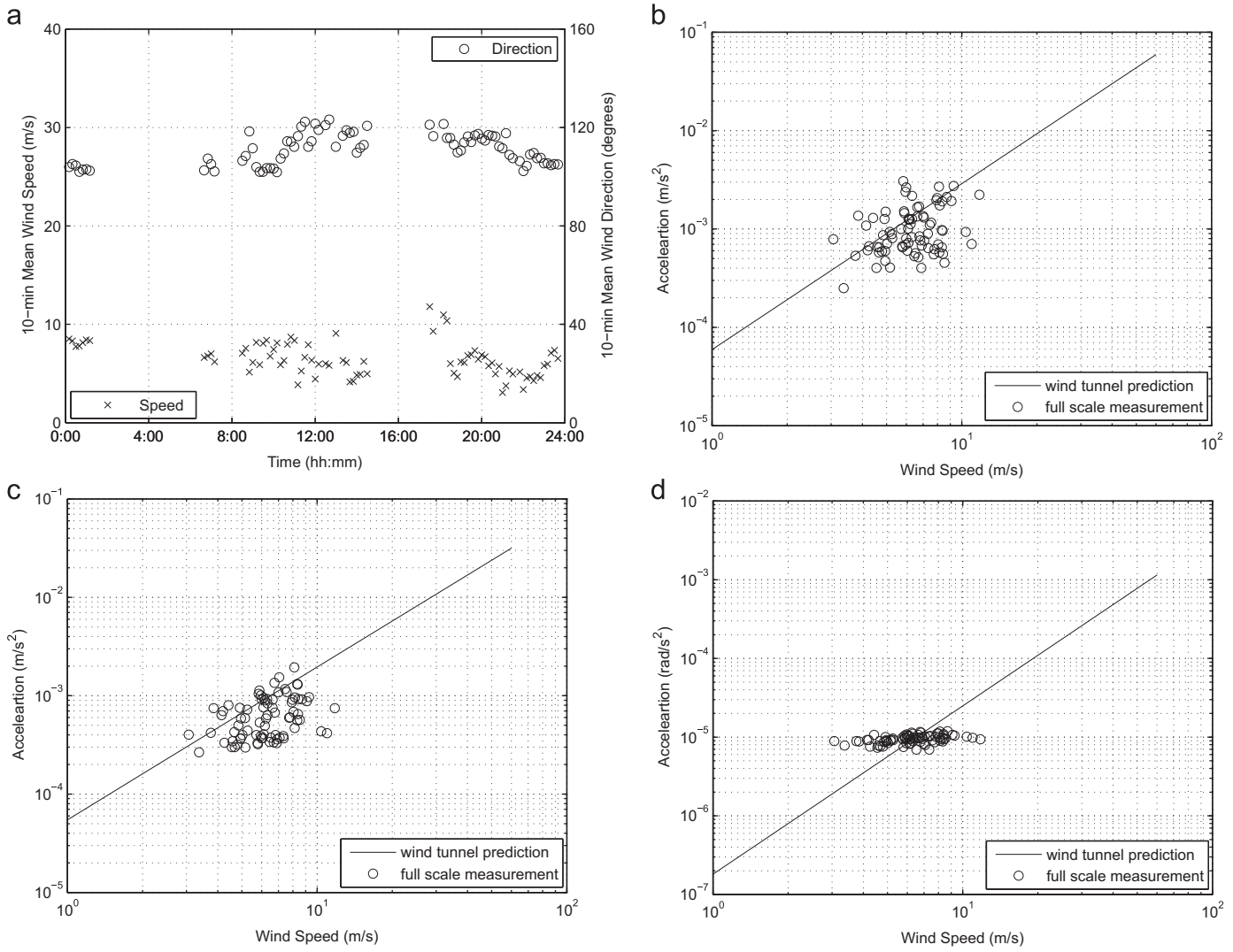

Fig. 10. Comparison between estimated RMS acceleration from wind tunnel test and measured RMS acceleration during Typhoon Nock-ten Typhoon Nock-ten, July 29, 2011: (a) selected 10-min mean wind speeds and wind directions, (b) *x*-direction, (c) *y*-direction, and (d) torsional direction.

while the RMS accelerations in torsional direction do not scatter much. The accelerations in *x*-direction are over-predicted in the wind tunnel; however, there is a reasonable match in the overall trend for *x*-direction, as shown in Fig. 9(b). For the *y*-direction, the predictions are much higher than the measured data, and the trend for the measurement data is steeper than the predicted trend, as shown in Fig. 9(c). It is seen in Fig. 9(d) that the match between measured acceleration and predicted acceleration for torsional direction is better than those for *x*- and *y*-directions, but the trend for the measurement data is flatter than the predicted trend. The level of comparison between the predicted and full scale data is influenced by the changing wind direction in full scale, variation in assumed damping values and a host of other parameters.

When comparing Fig. 10(b) with Fig. 9(b), Fig. 10(c) with Fig. 9(c), Fig. 10(d) with Fig. 9(d), it is noted that the predictions are more accurate for Typhoon Nock-ten than for Typhoon Haima. The prediction for *x*-direction is good (see Fig. 10(b)), while the prediction for *y*-direction is a slightly higher than most of the measured data (see Fig. 10(c)). A good match between prediction and measurement within the wind speed range 5–7 m/s is seen for torsional direction, but the predicted trend for torsional direction is not consistent (see Fig. 10(d)). One should note that the estimation of the tower responses for low wind speeds in the wind tunnel test also causes some scatter which reflects in the comparison.

It should be mentioned that the acceleration response corresponding to 10-year design wind speed govern the serviceability limit state design. The maximum acceleration from any wind direction for a 10-year design wind given in the wind tunnel test is 0.157 m/s^2, and it is about 20–36% lower than the serviceability (habitability) criteria used in North America (Isyumov and Kilpatrick, 1996), which is 20–25 milli-g (0.196–0.245 m/s^2) for office buildings in a 10-year event. So the serviceability requirement is satisfied according to wind tunnel test. The assessment of serviceability based on full-scale data will be addressed in Section 4.5.

4. Performance evaluation based on full-scale data

4.1. Stationarity analysis

Wind induced structural responses are usually considered as stationary random processes, however, in the real world they are not necessarily stationary due to some transient wind events, e.g. typhoons, thunderstorms and downbursts. Most of the output-only system identification methods have the assumption of stationarity. Thus in order to obtain reliable system identification

Table 1
Minimum percentage of data passing at least one stationarity test among different segments.

	Kammuri	Nuri	Hagupit	Molave	Koppu	Sarika	Haima	Nock-ten
Minimum percentage	93.75	93.75	85.71	18.75	91.67	64.29	88.89	94.44
Sections passed test	3/3	3/3	3/3	1/5	1/1	12/24	24/24	24/24

Table 2
Comparison of modal identification results obtained from different methods (Typhoon Haima).

Mode	frequency (Hz)					Damping ratio (%)				
	Design value	HPBW	RDT	FDD	c.o.v (%)	Design value	HPBW	RDT	FDD	c.o.v (%)
1	0.095	0.0917	0.0917	0.0917	0.04	1.50	0.63	0.55	0.53	9.54
2	0.139	0.1352	0.1376	0.1350	1.07	1.50	1.36	0.94	1.75	30.02
3	0.335	0.3726	0.3719	0.3722	0.10	1.00	0.85	0.85	0.52	25.34
4	0.345	0.4622	0.4630	0.4621	0.11	1.00	0.35	0.48	0.40	15.85
5	0.372	0.4976	0.4969	0.4978	0.10	–	0.37	0.12	0.26	50.01
6	0.452	0.5770	0.5776	0.5775	0.05	1.50	0.32	0.25	0.26	13.61
7	0.455	0.5993	0.5999	0.5993	0.06	–	0.10	0.17	0.16	26.85

Table 3
Comparison of modal identification results obtained from different methods (Typhoon Sarika).

Mode	frequency (Hz)					Damping ratio (%)				
	Design value	HPBW	RDT	FDD	c.o.v (%)	Design value	HPBW	RDT	FDD	c.o.v (%)
1	0.095	0.0920	0.0920	0.0919	0.04	1.50	0.52	0.35	1.43	75.88
2	0.139	0.1361	0.1390	0.1351	1.49	1.50	2.49	-0.88	2.46	142.72
3	0.335	0.3739	0.3747	0.3741	0.11	1.00	0.50	0.40	0.34	19.66
4	0.345	0.4634	0.4645	0.4636	0.13	1.00	0.31	0.65	0.29	48.98
5	0.372	0.4996	0.4996	0.4980	0.19	–	0.18	-0.02	0.70	129.32
6	0.452	0.5778	0.5778	0.5778	0.00	1.50	0.08	0.12	0.12	23.12
7	0.455	0.6010	0.6011	0.6010	0.01	–	0.17	0.15	0.53	75.97

results, the stationarity test must be conducted. In this paper, Run Test, Reverse Arrangements Test (Bendat and Piersol, 1986) and a check proposed by Montpellier (1996) are used to test the stationarity of acceleration data. The data are divided into one-hour segments for testing. For each segment, if more than 80% of data pass at least one stationarity test, this segment of data is considered as stationary data. Table 1 shows the minimum percentage of data passing at least one test and the number of segments passing the stationarity test among all tested segments for different typhoon events. Only one segment out of the total five tested segments passed the stationarity test for Typhoon Molave, and the minimum percentage of data passing at least one test was only 18.75%. This indicates that the acceleration responses induced by Typhoon Molave are non-stationary. For Typhoon Sarika, 12 out of the total 24 tested segments passed the stationarity test, and the minimum percentage of data passing at least one test was 64.29%. The responses measured during the other typhoon events passed the stationarity test.

4.2. Modal properties

Operational modal analysis has been studied by a number of investigators. A comparison of various output-only modal identification algorithms has been made by the authors by using the field measurement data of Canton Tower. The half power bandwidth (HPBW) (Bashor, 2011), random decrement technique (RDT) (Kijewski-Correa, 2003; Kijewski-Correa et al., 2006) and frequency domain decomposition (FDD) (Brincker et al., 2000; Carassale and Percivale, 2007) methods are used to identify the natural frequencies and damping ratios during different typhoon events; however, only the comparison results for Typhoon Haima and Typhoon Sarika are given in Table 2 and Table 3. As shown in Table 2, while the identified natural frequencies by using different methods are consistent, with the maximum coefficient of variation (c.o.v) 1.07% among the three methods, the identified damping ratios have much larger variations, with the maximum c.o.v 50.01%. The identified frequencies of the first two modes are slightly less than the design values, however, the identified damping ratios are much less than the design values. When comparing Table 3 with Table 2, it is seen that similarly as for Typhoon Haima, different methods give consistent results for frequency identification for Typhoon Sarika (the maximum c.o.v for natural frequencies is 1.49%), however, the identified damping ratios obtained by different methods have much larger discrepancies (the maximum c.o.v for damping ratios is 142.72%) than those of Typhoon Haima. The larger discrepancies are due to the fact that data measured during Typhoon Haima passed the stationary test, while 12 out of the total 24 tested segments for Typhoon Sarika did not pass the stationarity test. It is also worth noticing from Table 3 that the RDT gives negative damping ratios for Mode No. 2 and No. 5. This might be caused by aero-elastic effect. However, the HPBW and FDD methods cannot identify the negative damping, even if this is indeed the case.

Since this SHM system integrates the in-construction and in-service monitoring stages together, the structural responses during both stages have been measured. This offers us a unique opportunity to study the change in modal properties during construction. Table 4 shows the natural frequencies identified under different typhoon events during construction process. The results are obtained by using RDT. It is seen from Table 4 that the natural frequencies were decreasing as the construction progressed, since the structure became more slender. It is also noted

Table 4
Changes in natural frequencies during construction.

Mode	Design value	Kammuri (433.2 m)	Nuri (443.6 m)	Hagupit (448.8 m)	Molave (462.0 m)	Koppu (462.0 m)	Sarika (finished)	Haima (finished)	NockTen (finished)
1	0.905	0.1545	0.1427	0.1360	0.0980	0.0944	0.0920	0.0917	0.0917
2	0.139	0.2169	0.2031	0.1945	0.1442	0.1394	0.1390	0.1376	0.1344
3	0.335	0.4637	0.3426	0.4498	0.3674	0.3624	0.3747	0.3719	0.3722
4	0.345	0.5701	0.3956	0.5627	0.4206	0.4185	0.4645	0.4630	0.4617

Note: The unit of frequency is Hz. The heights of the main structure during construction are listed.

that the construction of the main structure had been almost finished when Typhoon Hagupit passed the area, noting that the height of main structure of the tower is about 450 m. The first natural frequency was about 0.1360 Hz during Typhoon Hagupit; while after finishing the antenna mast, the first natural frequency dropped to about 0.0917 Hz. This indicates the mast has a great influence on the natural frequencies of the whole structure. Consider the fact that the main structure is a concrete core with uniform cross-section, and it thus behaves like a giant cantilever. The addition of the mast, which is a steel lattice structure, significantly increased the total length of the cantilever by 35%. This caused a considerable reduction in the stiffness of the whole structure and thus resulted in a decrease in the fundamental frequency. Sometimes the addition of the mast can alter the dynamics of the combined system, resulting in new frequencies. If properly tuned, such masts can also serve as tuned mass dampers for the main tower.

4.3. Errors in modal identification

Due to the uncertainty in excitation and the wind environment, and the existence of measurement noises, the errors cannot be avoided in modal identification. The stationary white noise excitation is usually assumed in most out-put only modal identification methods (e.g. HPBW, FDD, and RDT). In practice, while normal ambient vibrations can be approximately treated as stationary, typhoons convecting past a structure are not necessarily stationary. When the excitations are non-stationary, the assumptions inherent to those algorithms are violated. As reported in Section 4.2, large discrepancies in damping ratio identified from different methods were observed when the data is non-stationary. Some other environmental factors, such as temperature, and construction activity may also affect the modal identification of results (Chen et al., 2011; Hua et al., 2007; Zhou et al., 2008).

The accuracy of HPBW method depends on the accuracy of PSD estimation. According to statistical theory, there exist two types of errors in PSD estimation: variance error (random error) and bias error (systematic error). The random error can be effectively reduced by computing PSD over n_d different blocks (data segments) and then averaging them. Random error in auto-spectral density estimate derived by Fast Fourier Transform (FFT) is given by (Bendat and Piersol, 1986)

$$e_r\left[\hat{S}_{xx}(f)\right]=\frac{1}{\sqrt{n_d}} \tag{6}$$

It is seen from Eq. (6) that as more averages are taken, the random error reduces. Bias is associated with the spacing of spectral lines. Having a frequency resolution Δf that is too coarse will smooth PSD peaks. Consequently, the spectral amplitude will be underestimated, while HPBW will be overestimated, resulting in an overestimated damping ratio. For closely spaced modes, the spectral bandwidth is also enhanced, which results in higher damping estimates (Pirnia et al., 2007). The normalized bias error is derived by using Taylor Series Expansion of power spectrum and is given by (Bendat and Piersol, 1986)

$$e_b\left[\hat{S}_{xx}(f_n)\right]\approx-\frac{1}{3}\left(\frac{\Delta f}{2\xi f_n}\right)^2 \tag{7}$$

where f_n is the natural frequency and ξ is the damping ratio. This formula is useful for determining frequency resolution when calculating PSD. It is common practice to insure that

$$\Delta f=\frac{2\xi f_n}{4} \tag{8}$$

This leads to a negligible bias error of approximately -2%. And the finer the frequency resolution is, the more accurate the estimation of HPBW becomes. In this study, an initial estimate of f_n and ξ ($f_n=0.09$ Hz, $\xi=1\%$) is used to determine the frequency resolution. The resulting minimum length of a block is about 44 min. To make the estimation more accurate, the length of a block used in this study is 88 min.

The RDT used in this study is proposed in Kijewski-Correa et al. (2006). Different vibration modes were filtered by using Butterworth filters. For each mode, data segments of prescribed length from the corresponding filtered time history that satisfies the trigger condition X_p are captured. The average of the captured segments is the random decrement signature (RDS). The RDT is inherently sensitive to the trigger conditions which directly influence the number of segments captured and due to the inherent randomness in the data quality of the RDS (Bashor, 2011). The reliability of the RDT can be improved through repeated triggering, as proposed in Kijewski-Correa (2003). This is achieved by generating several RDSs corresponding to different positive point triggers that are multiples of the standard deviation of the accelerations being analyzed ($X_p=M\sigma$). In this study, the triggers with $M=1, 1.5, 2, 2.5$ are used to generate RDSs. The modal frequencies and damping ratios are identified for each RDS. Then the average is taken as the estimation of modal frequencies and damping ratios. The length of the RDS is chosen as 20 cycles of the initial estimate of the first modal period (11.1 s).

4.4. Influence of vibration amplitude on modal properties

The vibration amplitude dependence in modal properties has been observed by a number of researchers (Kijewski-Correa et al., 2007; Kim et al., 2011; Li et al., 2003; Tamura and Suganuma, 1996; Wu et al., 2007). In this study, the change of modal frequencies and damping ratios with the change of RMS accelerations under winds is investigated. The acceleration responses measured during Typhoon Haima and Typhoon Nock-ten are analyzed, since both of them passed the stationary test and data quantity of them is enough. The 23-h data measured during Typhoon Haima and 24-h data measured during Typhoon Nock-ten are used in this analysis. The RDT is employed to identify the amplitude-dependent modal properties. The accelerations are divided into 1-h segments, and the RMS, and natural frequencies, damping ratios are extracted for each segment. Considering the fact that the vibration of this structure is highly coupled in both

x- and y-directions, both the x- and y-direction responses are used for modal identification of each mode. Since the higher order modal responses are modest comparing to the ambient noise, the identified higher order modal parameters, especially the damping ratio, become questionable. Thus only the first two modes are used to study the amplitude-dependent modal properties. The relationship between the identified natural frequencies and RMS accelerations for the first two modes are shown in Fig. 11. When the vibration amplitude increases, a generally decreasing trend in natural frequencies can be observed for both modes. In order to approximately model the relationship between the frequencies and RMS accelerations, a linear regression model is used and expressed as follows.

$$f = \alpha_0 x + \alpha_1 \tag{9}$$

where f is the natural frequency in Hz, x is the RMS acceleration in 10^{-3} m/s^2, α_0 and α_1 are the regression coefficients. The fitted lines are shown in Fig. 11 and the coefficients of the linear representation are given in Table 5. When comparing Fig. 11(a, b) with Fig. 11(c, d), it is seen that the frequency amplitude dependence for the first mode follows the linear fitted line better, especially in the low amplitude range (below 2.5×10^{-3} m/s^2 for x-direction and 2×10^{-3} m/s^2 for y-direction), than that for the second mode. Although the identified frequencies scatter around the fitted line, the degree of frequency amplitude-dependence can be described by the coefficient α_0. When comparing α_0 for the first and second modes in Table 5, it is found that the frequency of the second mode decreased more than that of the first mode with the increase of amplitude.

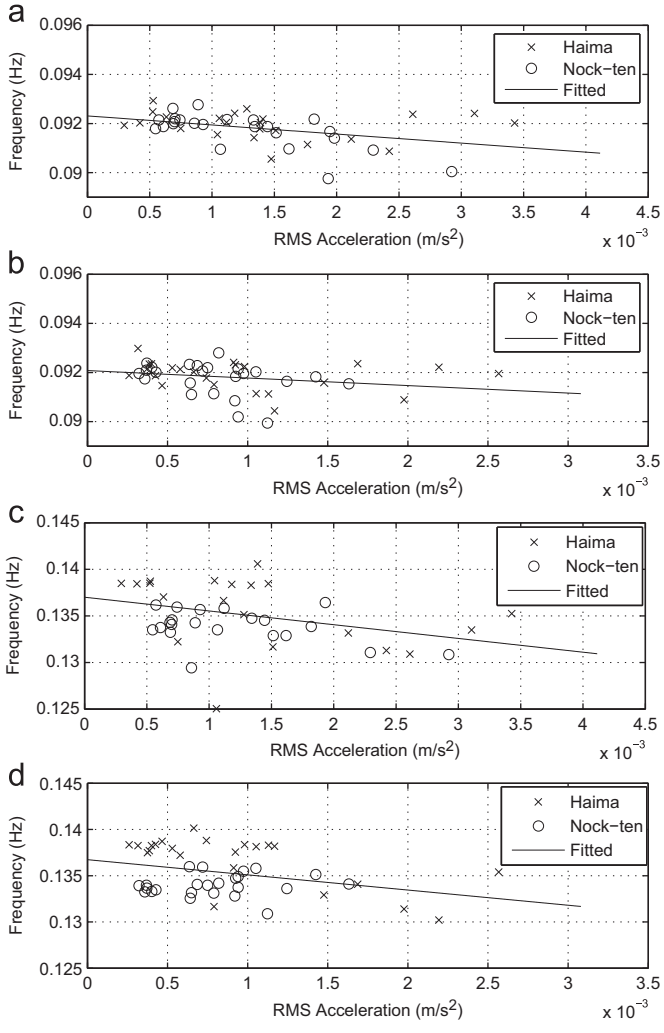

Fig. 11. Relationship between frequency and RMS acceleration: (a) frequency of 1st mode identified from x-direction acceleration, (b) frequency of 1st mode identified from y-direction acceleration, (c) frequency of 2nd mode identified from x-direction acceleration, and (d) frequency of 2nd mode identified from y-direction acceleration.

Table 5
Coefficients of linear representation of frequency amplitude dependence.

Mode	x-direction		y-direction	
	$\alpha_0(10^3\cdot(\mathrm{m/s})^{-1}\cdot\mathrm{Hz})$	α_1(Hz)	$\alpha_0(10^3\cdot(\mathrm{m/s})^{-1}\cdot\mathrm{Hz})$	α_1(Hz)
1	−0.000369	0.000092	−0.000305	0.000092
2	−0.001475	0.000137	−0.001642	0.000137

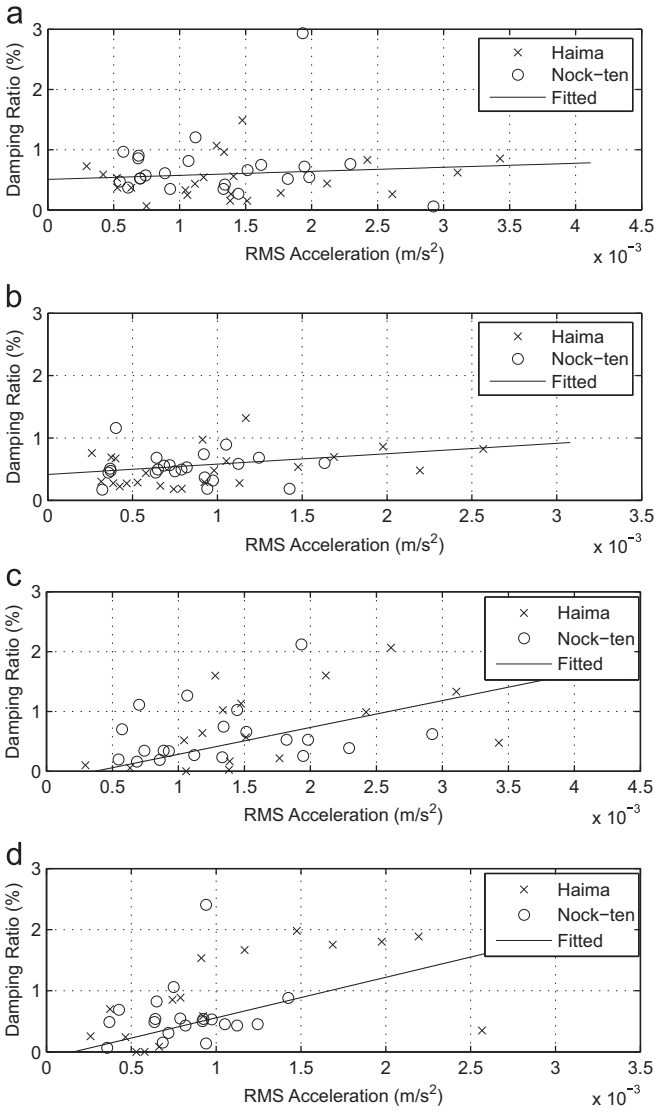

Fig. 12. Relationship between damping ratio and RMS acceleration: (a) damping ratio of 1st mode identified from x-direction acceleration, (b) damping ratio of 1st mode identified from y-direction acceleration, (c) damping ratio of 2nd mode identified from x-direction acceleration, and (d) damping ratio of 2nd mode identified from y-direction acceleration.

The relationship between the identified damping ratio and RMS accelerations for the first two modes are also studied. As shown in Fig. 12, the identified damping ratio increased when the RMS accelerations increased for both modes. Similar to the

Table 6
Coefficients of linear representation of damping amplitude dependence.

Mode	x-direction		y-direction	
	$\beta_0(10^3\cdot(\mathrm{m/s})^{-1}\cdot\%)$	$\beta_1(\%)$	$\beta_0(10^3\cdot(\mathrm{m/s})^{-1}\cdot\%)$	$\beta_1(\%)$
1	0.066827	0.000508	0.166487	0.000414
2	0.448534	−0.000165	0.662895	−0.000106

frequency amplitude-dependence, linear regression is used to model the relationship. The model is given by

$$\xi = \beta_0 x + \beta_1 \tag{10}$$

where ξ is the damping ratio in %, x is the RMS acceleration in 10^{-3} m/s^2, β_0 and β_1 are the regression coefficients. The fitted lines are shown in Fig. 12 and the coefficients of the linear representation are given in Table 6. The linear relationship approximates the damping amplitude dependence for the first mode better than for the second mode. It is also seen from Fig. 12 and Table 6 that the amplitude-dependence in damping ratio for the second mode is much larger than that for the first mode.

The core of the tower is made of reinforced concrete. The damping of the tower will include contributions from material damping, external friction damping, and aerodynamic damping. Material damping is in general given by internal friction between microscopic and macroscopic structure of the material and along the cracked concrete surfaces. For low wind speeds, such as those of the present study, it is likely that most of the observed damping results from the material damping. This will work in tandem with other macroscopic frictional damping sources such as the interfaces of the partition walls with framing (external friction damping). For larger wind speeds, the amplitude of vibration will presumably become larger. This is likely to initiate dissipative mechanisms due to slippage along cracked internal surfaces of the concrete and other internal frictions, consequently, increasing the material damping and therefore the total damping of the structure. It is generally accepted that there will be a certain flattening (low amplitude plateau) of the damping values before the vibration amplitudes are large enough to initiate slippage at cracked locations and other internal friction mechanisms. Due to the low wind speeds, the data presented in this paper probably falls in the aforementioned low amplitude region. It is therefore likely that for higher vibration amplitudes a certain increase in damping will be observed. Concerning the aerodynamic damping, for tower shaped structures, this is usually small compared to damping from other sources and is generally positive in the along-wind direction while assuming negative values in the across-wind direction above certain wind speeds. The aerodynamic damping in the along-wind direction is expected to increase with wind speed according to the quasi-steady theory. This might explain why the amplitude-dependence in the damping ratio identified from the y-direction responses is generally larger than that identified from the x-direction responses (see Table 6, β_0 for y-direction is larger than that for the x-direction for both modes), keeping in mind that the y-direction is close to the along-wind direction.

4.5. Serviceability (habitability) assessment

Table 7 shows the maximum wind speeds and accelerations during eight typhoon events. The peak accelerations are much smaller than the serviceability criteria used in North America (Isyumov and Kilpatrick, 1996), which is 20–25 milli-g (0.196–0.245 m/s^2) for office buildings in a 10-year event. Since the measured wind speeds in the eight typhoon events are smaller than the 10-year design wind speed due to their respective paths and intensities, a linear regression is used to predict the maximum acceleration at the 10-year design wind speed (3-s wind speed of 38.7 m/s) based on the data given in Table 7. The estimated maximum acceleration for a 10-year wind event is 0.0503 m/s^2. If a 90% confidence interval of the prediction is used, the estimation will be within the range 0.0160–0.1577 m/s^2. The upper limit of the 90% confidence interval is 20% less than the serviceability criteria (20 milli-g used). Therefore, if a 90% confidence interval is used, the design serviceability limit state of the tower is satisfied. However, the performance may be significantly impacted should a typhoon of a stronger intensity move by closer to the tower. It is also worth noting that while evaluating serviceability in typhoon events and especially in tower-type structures with usage that differs from office and residence, consideration should be given to the frequency of such events and standard regarding the usage of such facilities during extreme winds.

Table 7
Maximum 3-s wind speed and acceleration responses during typhoons.

Typhoon	Time	Max. 3-s wind speed	Max. Acc		Height[a] (m)
			(m/s^2)	(milli-g)	
Kammuri	August 6, 2008	32.3	0.0197	2.01	384.2
Nuri	August 22, 2008	25.5	0.0199	2.03	332.2
Hagupit	September 24, 2008	34.6	0.0414	4.22	384.2
Molave	July 18, 2009	29.7	0.0818	8.35	332.2
Koppu	September 15, 2009	28.0	0.0508	5.19	446.8
Sarika	June 10, 2011	9.7	0.0089	0.91	275.3
Haima	June 22, 2011	17.6	0.0164	1.67	446.8
Nock-ten	July 29, 2011	16.8	0.0197	2.01	446.8

[a] The height at which the maximum acceleration was measured.

5. Conclusions

This paper evaluates the performance of Canton Tower during typhoon events based on full-scale data. The measured wind properties, such as wind speed, direction during Typhoon Sarika, Typhoon Haima and Typhoon Nock-ten, as well as the turbulence intensity of Typhoon Haima are reported. The measured structural dynamic responses (acceleration, displacements, and strain) are analyzed. The maximum stress variation during Typhoon Neoguri, Typhoon Kammuri, Typhoon Nuri, and Typhoon Hagupit was approximately 0.5 MPa, which was about 20% of the static stress produced by the self-weight of the structure, while the maximum displacement during these four typhoon events was about 15 cm. The maximum accelerations for Typhoon Hagupit, Typhoon Haima and Typhoon Nock-ten occurred in x-direction, suggesting that the structural stiffness in the y-axis is generally greater than that in the x-axis, resulting in dominant responses in x-axis. Comparison of PSD of accelerations measured at different levels during Typhoon Haima reveals that the lower order modes were dominant in the response at higher levels of the tower, and the higher order modes became dominant in the responses of lower levels. The PSD of displacements measured by GPS showed consistency with the PSD of accelerations, however, the PSD of accelerations exhibit more peaks in high frequency range as expected, from which the higher modes of the structure could be identified. The wind tunnel test results are compared with the full-scale data. The predictions are generally more consistent for Typhoon Nock-ten than for Typhoon Haima.

A comparative study of modal properties identification by using different methods (i.e. HPBW, RDT and FDD) is conducted. The modal frequencies in different construction stages are

compared. Some issues affecting the accuracy of modal identification have been addressed. The vibration amplitude-dependence in modal properties is investigated. A decreasing trend in modal frequencies and an increasing trend in damping ratios with the increase of vibration amplitude have been observed, which has been noted by others in buildings. The tower serviceability during typhoon events is also evaluated and the performance is found to be satisfactory if a 90% confidence interval is used for prediction.

Acknowledgments

The work described in this paper was supported in part by a grant from the Research Grants Council of the Hong Kong Special Administrative Region, China (Project no. PolyU 5280/09E). Support for data analysis and modeling has been provided by NSF Grant CMMI 09-28282 and Global Center of Excellence at Tokyo Polytechnic University, funded by MEXT. The authors appreciate the help and suggestions provided by Dr. L. Carassale, University of Genoa, in the analysis of data. The authors are also grateful to Mr. Lixiao Li and Dr. Seymour Spence of the University of Notre Dame for their suggestions and help regarding paper revision.

References

Bashor, R.E., 2011. Dynamics of wind sensitive structures. Ph.D. Dissertation. University of Notre Dame, Notre Dame.

Bendat, J.S., Piersol, A.G., 1986. Random Data: Analysis and Measurement Procedures, second ed. John Wiley & Sons, Inc., New York.

Brincker, R., Zhang, L., Andersen, P., 2000. Modal identification from ambient responses using frequency domain decomposition, in: Proceedings of the 18th International Modal Analysis Conference, pp. 625–630.

Carassale, L., Percivale, F., 2007. POD-based modal identification of wind-excited structures, in: Proceedings of the 12th International Conference on Wind Engineering, pp. 1239–1246.

Chen, W.H., Lu, Z.R., Lin, W., Chen, S.H., Ni, Y.Q., Xia, Y., Liao, W.Y., 2011. Theoretical and experimental modal analysis of the Guangzhou New TV Tower. Engineering Structures 33, 3628–3646.

GBJ9-Department of Standards and Norms, 1994. Load Code for the Design of Building Structures (English Translation). New World Press, Beijing.

Hua, X.G., Ni, Y.Q., Ko, J.M., Wong, K.Y., 2007. Modeling of temperature-frequency correlation using combined principal component analysis and support vector regression technique. Journal of Computing in Civil Engineering 21, 122–135.

Huang, M.J., 2006. Utilization of strong-motion records for post-earthquake damage assessment of buildings, in: Proceedings of the International Workshop on Structural Health Monitoring and Damage Assessment, pp. IV1–IV29.

Isyumov, N., Kilpatrick, J., 1996. Full-Scale Experience with Wind-Induced Motions of Tall Buildings, Tall Building and Structures. Council on Tall Buildings and Urban Habitat.

Kijewski-Correa, T., 2003. Time-frequency perspectives in system identification: from theory to full-scale measurement. Ph.D. Dissertation. University of Notre Dame, Notre Dame.

Kijewski-Correa, T., Kareem, A., 2003. The Chicago monitoring project: a fusion of information technologies and advanced sensing for civil infrastructure. In: Wu, Z.S., Abe, M. (Eds.), Structural Health Monitoring and Intelligent Infrastructure. Balkema, Lisse, pp. 1003–1010.

Kijewski-Correa, T., Kilpatrick, J., Kareem, A., Kwon, D.-K., Bashor, R., Kochly, M., Young, B.S., Abdelrazaq, A., Galsworthy, J., Isyumov, N., Morrish, D., Sinn, R.C., Baker, W.F., 2006. Validating wind-induced response of tall buildings: synopsis of the Chicago full-scale monitoring program. Journal of Structural Engineering 132, 1509–1523.

Kijewski-Correa, T., Prinia, J.D., Bashor, R.E., Kareem, A., Kilpatrick, J., Brad, Y., Galsworthy, J., Isyumov, N., Morrish, D., Baker, W., 2007. Full-scale performance evaluation of tall buildings under winds, in: Proceedings of the 12th International Conference on Wind Engineering, pp. 351–358.

Kim, J.Y., Yu, E., Kim, D.Y., Tamura, Y., 2011. Long-term monitoring of wind-induced responses of a large-span roof structure. Journal of Wind Engineering and Industrial Aerodynamics 99, 955–963.

Li, Q.S., Wu, J.R., Liang, S.G., Xiao, Y.Q., Wong, C.K., 2004. Full-scale measurements and numerical evaluation of wind-induced vibration of a 63-story reinforced concrete tall building. Engineering Structures 26, 1779–1794.

Li, Q.S., Xiao, Y.Q., Wu, J.R., Fu, J.Y., Li, Z.N., 2008. Typhoon effects on super-tall buildings. Journal of Sound and Vibration 313, 581–602.

Li, Q.S., Yang, K., Wong, C.K., Jeary, A.P., 2003. The effect of amplitude-dependent damping on wind-induced vibrations of a super tall building. Journal of Wind Engineering and Industrial Aerodynamics 91, 1175–1198.

Lin, C.C., Wang, C.E., Wang, J.F., 2003. On-line building damage assessment based on earthquake records. In: Wu, Z.S., Abe, M. (Eds.), Structural Health Monitoring and Intelligent Infrastructure. Balkema, Lisse, pp. 551–559.

Montpellier, P.R., 1996. The maximum likelihood method of estimating dynamic properties of structures, Department of Civil Engineering. Master Dissertation. University of Western Ontario, London.

Ni, Y.Q., Wong, K.Y., Xia, Y., 2011. Health checks through landmark bridges to sky-high structures. Advances in Structural Engineering 14, 103–119.

Ni, Y.Q., Xia, Y., Liao, W.Y., Ko, J.M., 2009. Technology innovation in developing the structural health monitoring system for Guangzhou New TV Tower. Structural Control and Health Monitoring 16, 73–98.

Pasquill, F., 1974. Atmospheric Diffusion, second ed. John Wiley & Sons, Inc., New York.

Pirnia, J.D., Kijewski-Correa, T., Abdelrazaq, A., Chung, J., Kareem, A., 2007. Full-scale validation of wind-induced response of tall buildings: investigation of amplitude-dependent dynamic properties, in: Proceedings of the Structures Congress 2007. ASCE.

Tamura, Y., Suganuma, S., 1996. Evaluation of amplitude-dependent damping and natural frequency of buildings during strong winds. Journal of Wind Engineering and Industrial Aerodynamics 56, 115–130.

Wu, J.R., Fu, J.Y., Xu, A., Li, Q.S., Xiao, Y.Q., 2011. Field measurements of wind characteristics and wind effects on Guangzhou West Tower, in: Proceedings of the 13th International Conference on Wind Engineering.

Wu, J.R., Liu, P.F., Li, Q.S., 2007. Effects of amplitude-dependent damping and time constant on wind-induced responses of super tall building. Computers & Structures 85, 1165–1176.

Xu, Y.L., Zhan, S., 2001. Field measurements of Di Wang Tower during Typhoon York. Journal of Wind Engineering and Industrial Aerodynamics 89, 73–93.

Zhou, H.F., Ni, Y.Q., Ko, J.M., Wong, K.Y., 2008. Modeling of wind and temperature effects on modal frequencies and analysis of relative strength of effect. Wind and Structures 11, 35–50.

Zhu, L.D., Ding, Q.S., Chen, W., 2006. Wind tunnel test of aeroelastic full model of Guangzhou New TV Tower. Report. State Key Laboratory of Disaster Reduction in Civil Engineering, Tongji University, Shanghai (in Chinese).

Zhu, L.D., Ding, Q.S., Tan, X., Wen, S.B., 2007. Aeroelastic model test of a 610 m-high TV tower in Guangzhou City of China, in: Proceedings of the 12th International Conference on Wind Engineering, pp. 975–982.